Electronic Supplementary Material (ESI) for Journal of Materials Chemistry A.

Supporting Information

Insight into the Role of Ni-Fe Dual Sites towards Oxygen Evolution Reaction Based on Atomically Metal-Doped Polymeric Carbon Nitride

Chuchu Wu,[ab] Xiaoming Zhang,[a] Zhangxun Xia,[a] Miao Shu,[bc] Huanqiao Li,[a] Xinlong Xu,[ab] Rui Si,[c] Alexandre I. Rykov,[d] Junhu Wang,[d] Shansheng Yu,[e] Suli Wang,*[a] and Gongquan Sun*[a]

[a] Dalian National Laboratory for Clean Energy, Dalian Institute of Chemical Physics, Chinese Academy of Sciences, Dalian 116023, China

[b] University of Chinese Academy of Sciences, Beijing, 100049, China

[c] Shanghai Synchrotron Radiation Facility, Shanghai Institute of Applied Physics, Chinese Academy of Sciences, Shanghai, 201204, China

[d] Mössbauer Effect Data Center, Dalian Institute of Chemical Physics, Chinese Academy of Sciences, Dalian 116023, China

[e] Department of Materials Science, Jilin University, Changchun 130012, China

I. Supplemental Figures

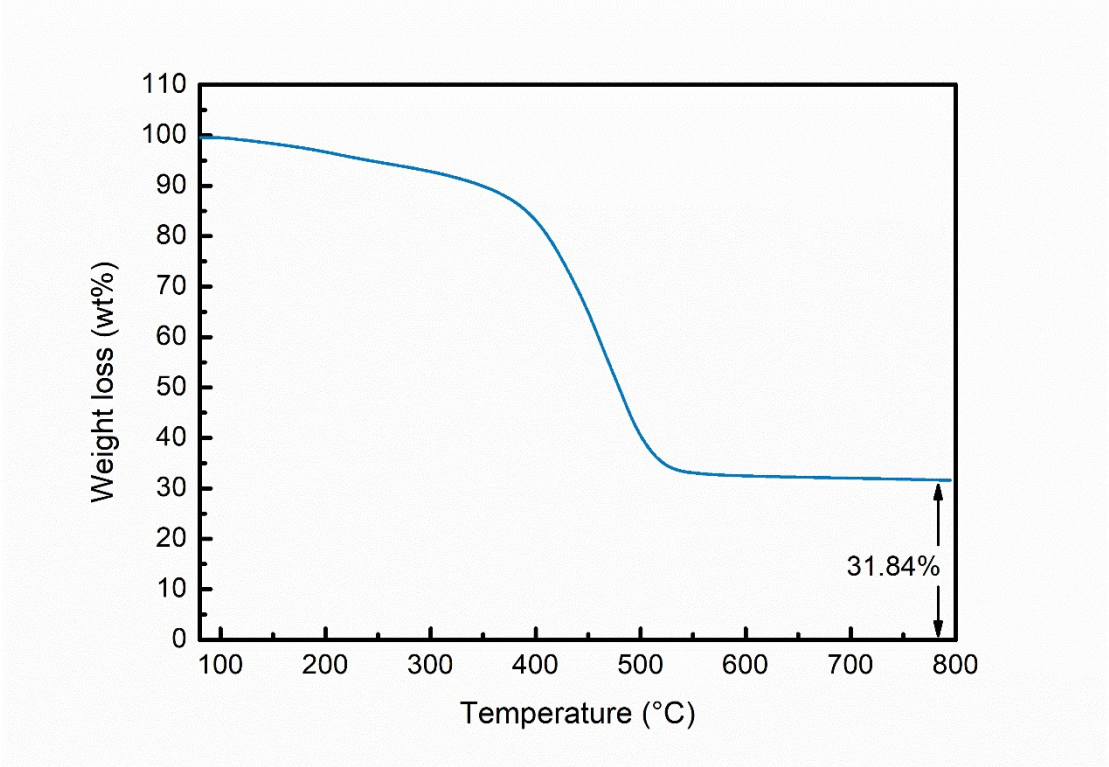

Figure S1. Thermogravimetric analysis of $Ni_{0.65}Fe_{0.35}$@PCN.

Thermogravimetric analysis was carried out under air atmosphere to 800°C, and the amount of inorganic residue is 31.84 wt%. At 800°C, nickel species has been oxidized to NiO. Taking the loading content on the pristine sample into consideration (Ni: 15.36 wt%; Fe: 8.82 wt%), the amount of inorganic residue is about 31.74 wt% assuming the product of iron species is Fe_3O_4, and about 32.16 wt% assuming the product is Fe_2O_3. The calculated value is close to the experimental result of TGA, further confirming the atomic metal components.

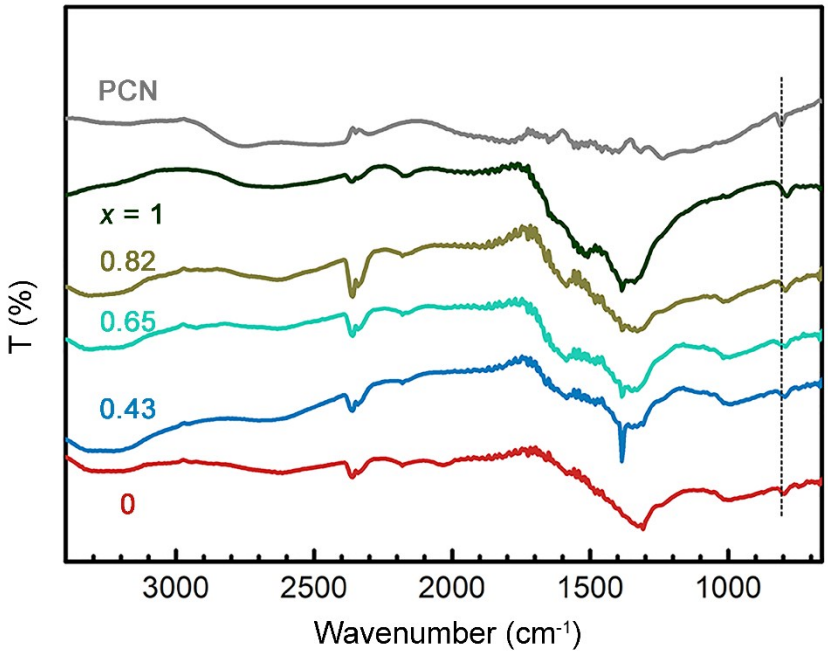

Figure S2. FT-IR transmittance spectra of PCN and Ni_xFe_{1-x}@PCN.

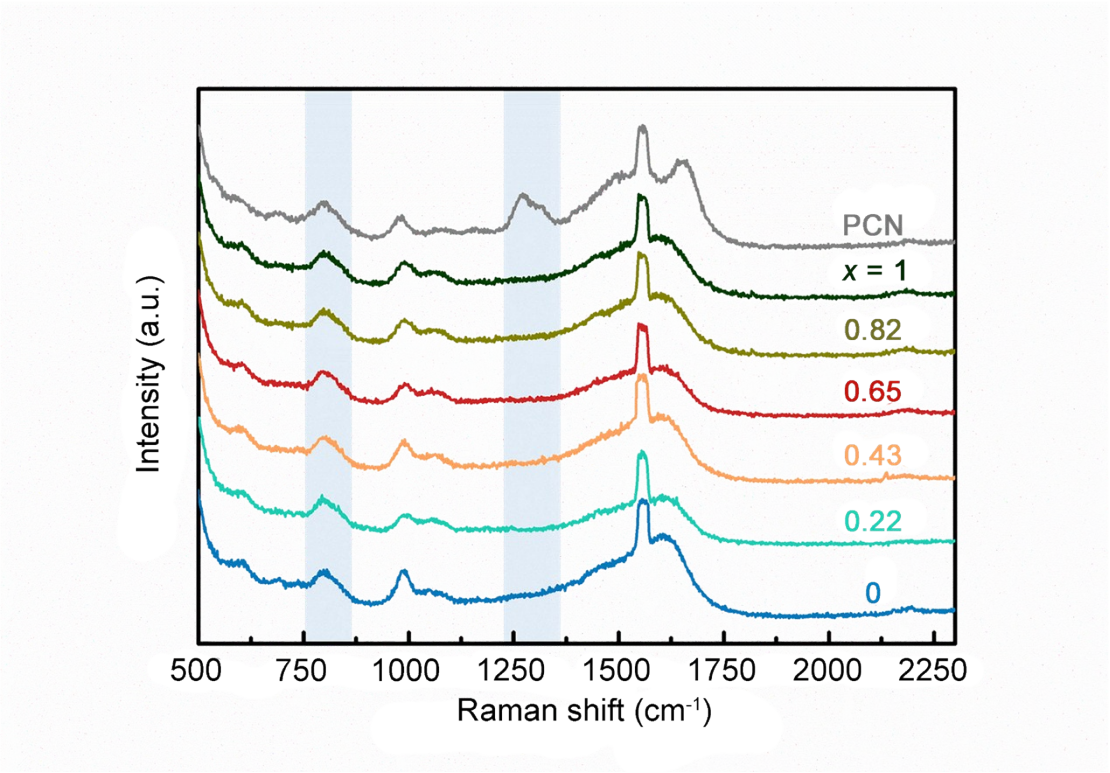

Figure S3. Raman spectra of PCN and Ni_xFe_{1-x}@PCN.

We were unable to make a tentative assignment of the peak at 1268 cm^{-1} in PCN, which disappears after introducing metal. However, according to the range it appears, it might be attributed to the vibration mode of nitrogenous component of PCN, intensity of which decreased dramatically after metal doping because metal is coordinated with N atoms. The strong peak around 1557 cm^{-1} is attributed to oxygen in air.

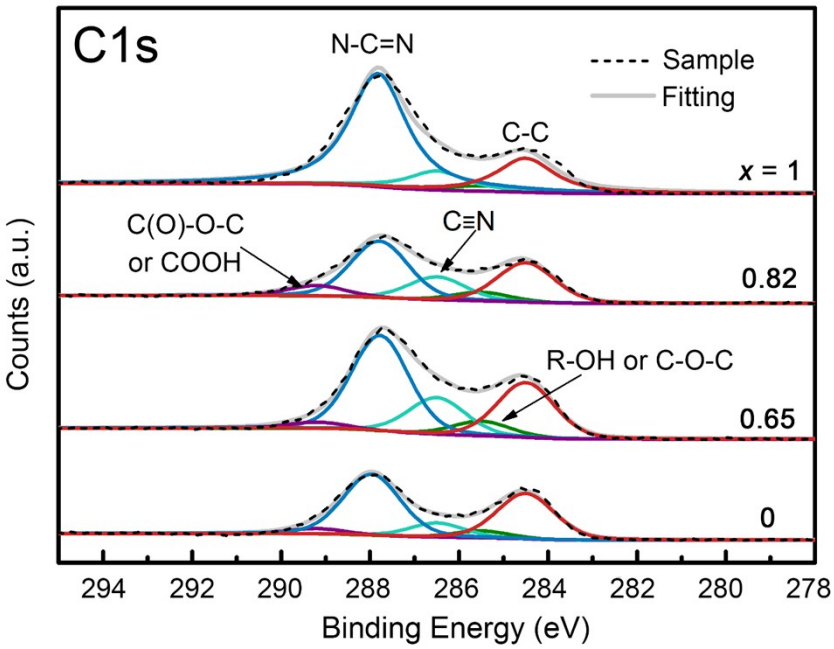

Figure S4. C 1s high-resolution XPS surveys of Ni_xFe_{1-x}@PCN.

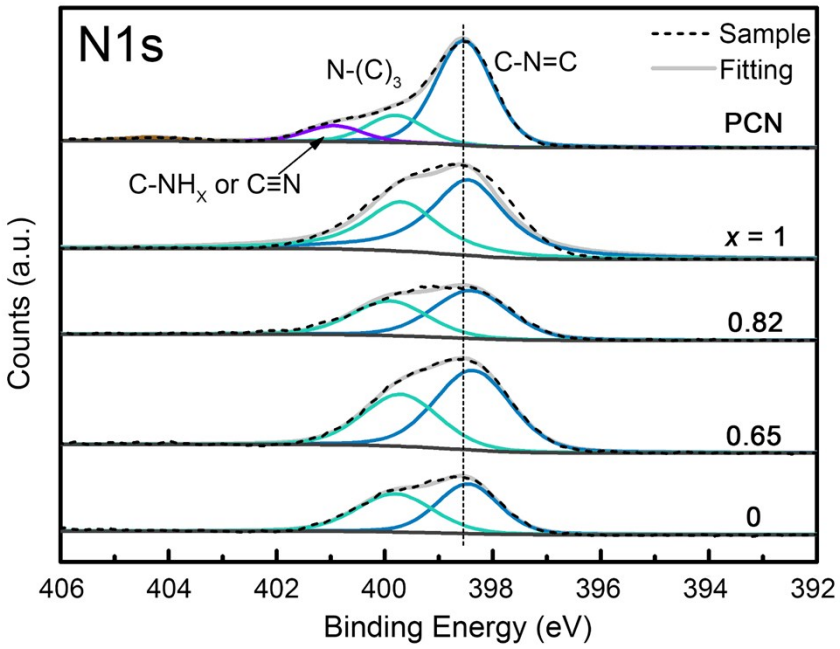

Figure S5. N 1s high-resolution XPS surveys of PCN and Ni_xFe_{1-x}@PCN.

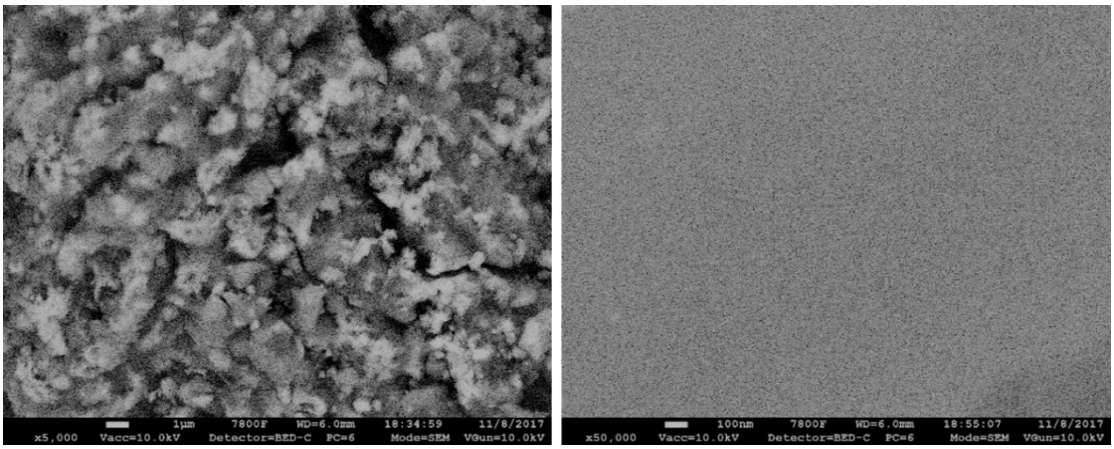

Figure S6. SEM image of $Ni_{0.65}Fe_{0.35}$@PCN under the back scattered electron mode

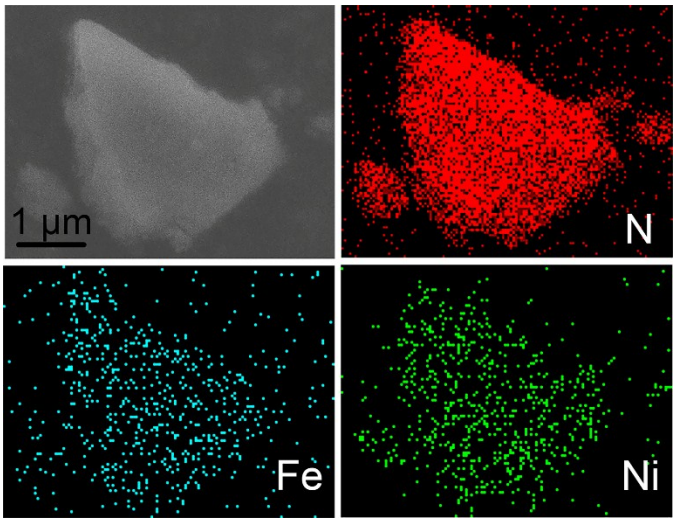

Figure S7. SEM image of $Ni_{0.65}Fe_{0.35}$@PCN as well as corresponding EDS mapping images of N, Fe and Ni.

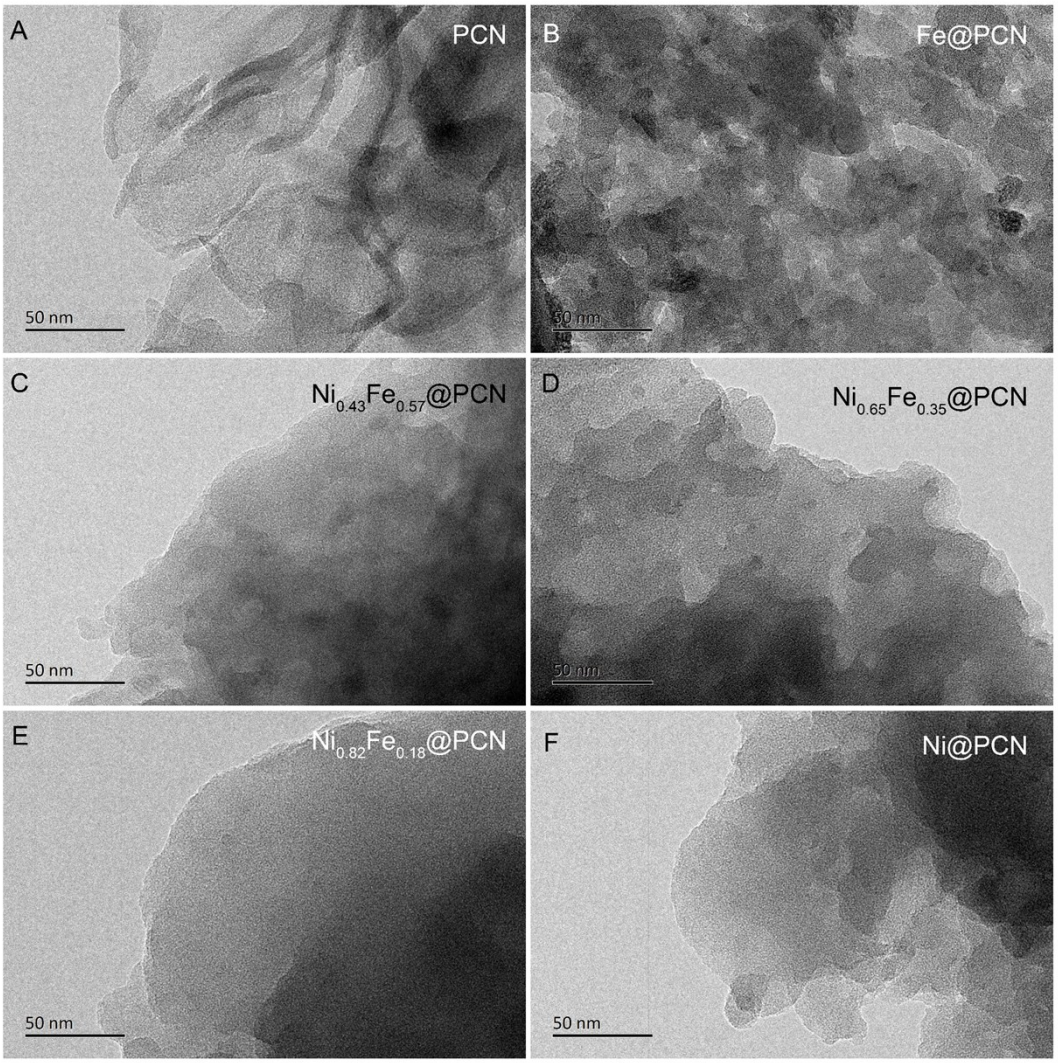

Figure S8. TEM images of PCN (A), Fe@PCN (B), $Ni_{0.43}Fe_{0.57}$@PCN (C), $Ni_{0.65}Fe_{0.35}$@PCN (D), $Ni_{0.82}Fe_{0.18}$@PCN (E), and Ni@PCN (F).

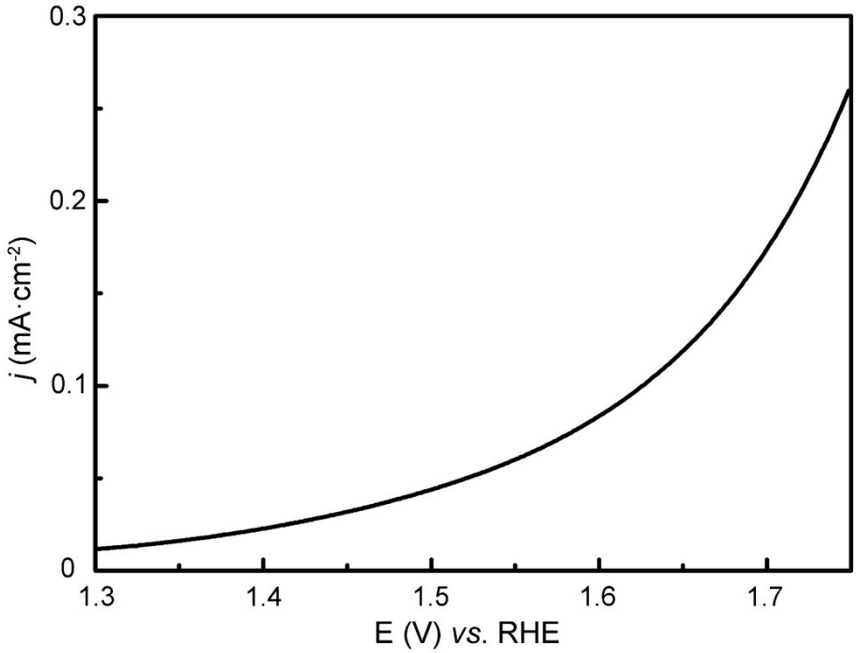

Figure S9. OER polarization curves of mixture of PCN and Vulcan XC-72 in O_2-satuated 1 M KOH. Scan rate: 10 mV/s, electrode rotation rate: 1600 rpm.

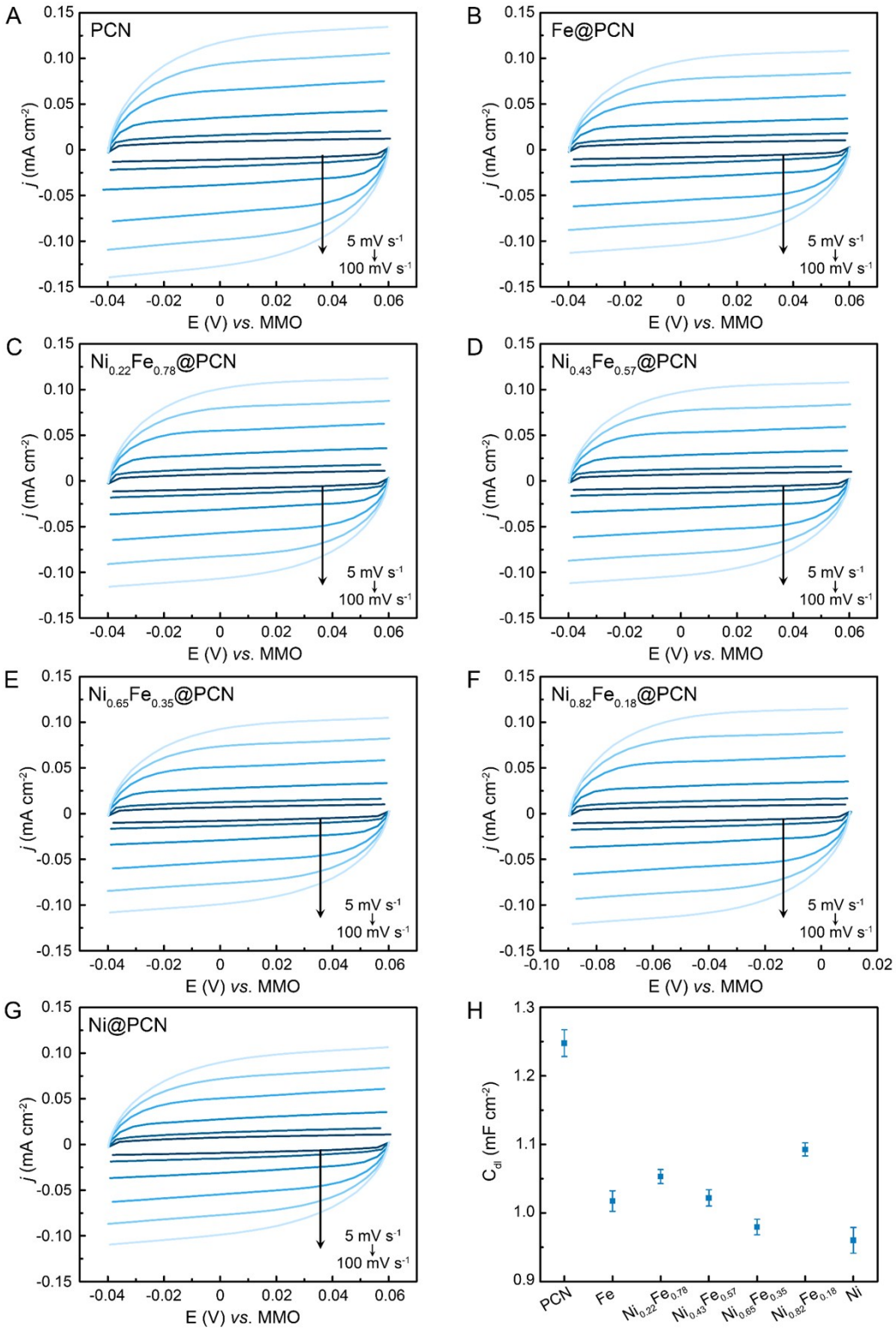

Figure S10. The electric double layer capacitance (C_{dl}) measurements of PCN and Ni_xFe_{1-x}@PCN.

The electrochemically active surface area (ECSA) is calculated on the basis of measured double-layer capacitance using LSVs in a non-Faradaic potential range, typically a 0.1 V window around OCP. LSV measurements were conducted in a quiescent solution of 1M KOH by sweeping the potential anodically or cathodically at 6 different scan rates: 0.005, 0.01, 0.025, 0.05, 0.075 and 0.1 $V \cdot s^{-1}$. The working electrode was held at each potential vertex for 10 s before beginning the next sweep. The electrical double layer capacitance (C_{dl}) was obtained by calculating the slope from the linear relationship of the current density against the scan rate, and the results were shown on Figure S10H. The larger C_{dl} value of PCN is due to the two-dimensional morphology (See Figure S8A), which is partly destroyed when metal ions are introduced.

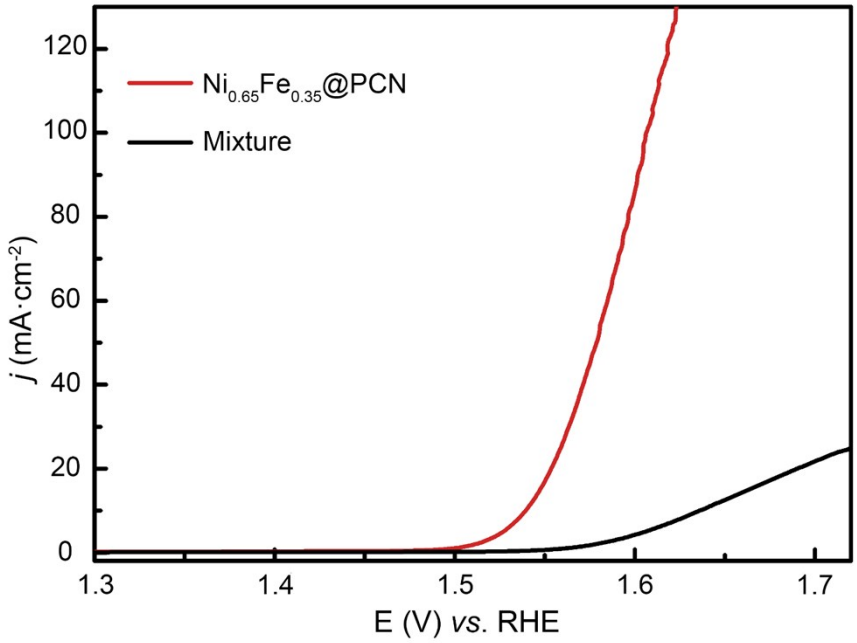

Figure S11. OER polarization curves of mixture of Ni@PCN and Fe@PCN (mass ratio 1:1) as well as $Ni_{0.65}Fe_{0.35}$@PCN in O_2-satuated 1 M KOH. Scan rate: 10 mV/s, electrode rotation rate: 1600 rpm.

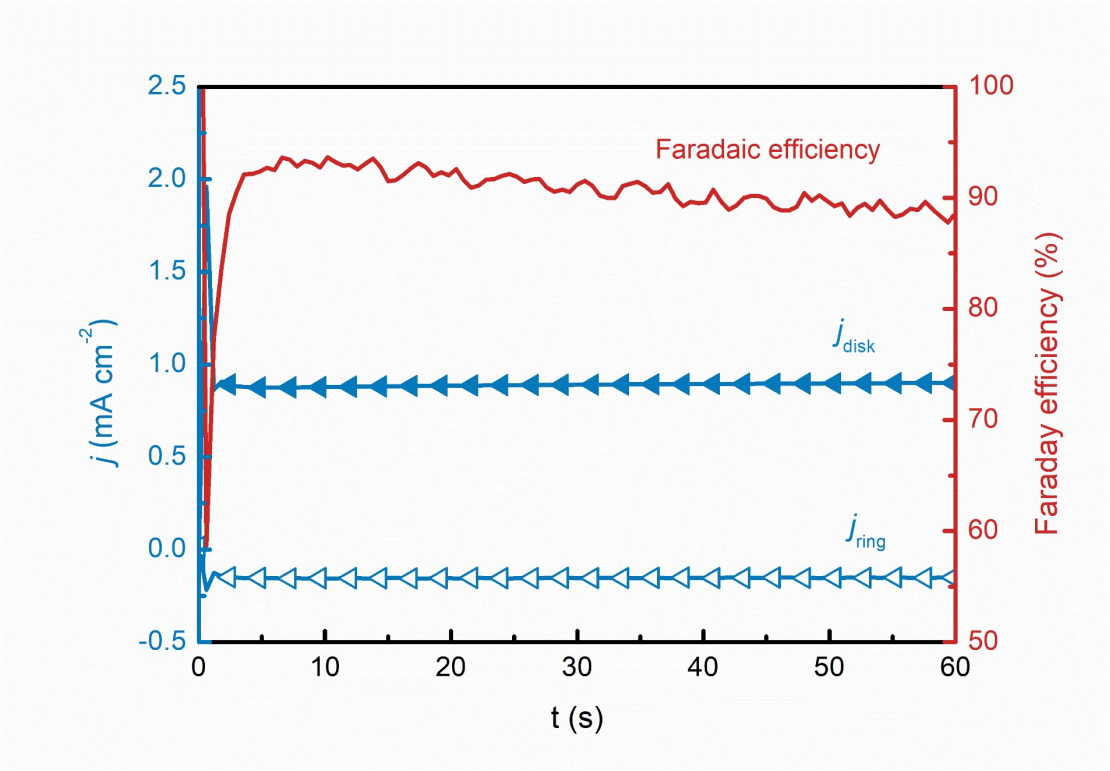

Figure S12. Faradaic efficiency testing of $Ni_{0.65}Fe_{0.35}$@PCN using the RRDE technique in N_2-saturated 1 M KOH solution.

When a constant potential (1.493 V vs. RHE) is applied to the glassy-carbon disk electrode (0.255 cm^2) for oxygen generation, a ring current caused by oxygen reduction is detected immediately. The Pt ring electrode was held at a constant potential E = 0.3 V vs RHE to rapidly reduce O_2 to H_2O_2. The disk current density is below 1 $mA \cdot cm^{-2}$ which is sufficiently large to ensure appreciable O_2 production but sufficiently small to minimize local saturation and bubble formation at the disk electrode. The electrode rotation rate is kept 1200 rpm so that the apparent number of electron transfer, n_{app} = *ca.* 2. The Faradaic efficiency of the OER system, ε, is proportional to the ratio of the ring current to the disk current and is given by the equation below:

$$\varepsilon = \frac{2i_r}{i_d N}$$

where i_r is the measured ring current, i_d is the measured disc current, and N = 0.38 is the collection efficiency for the RRDE.

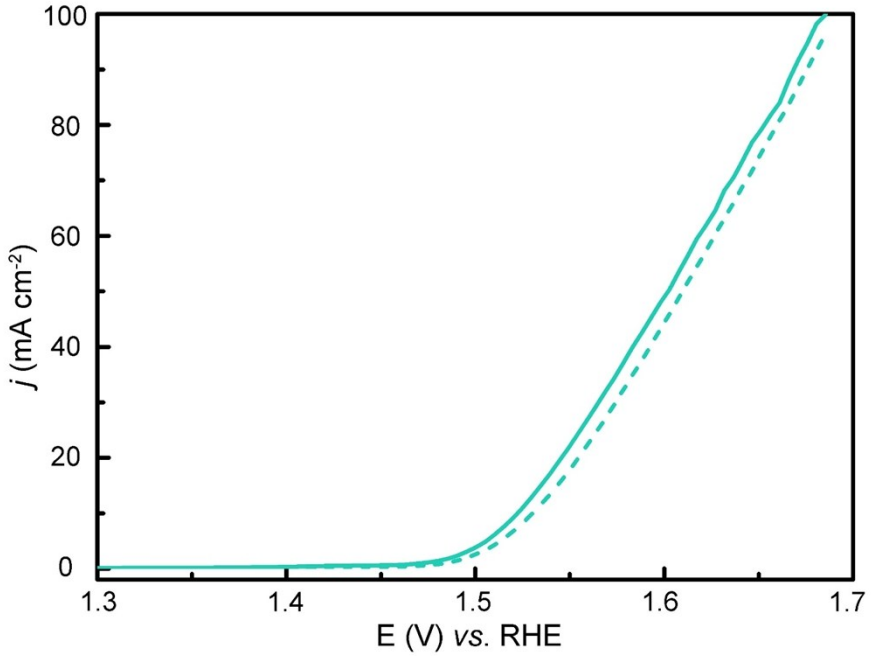

Figure S13. OER polarization curves of $Ni_{0.65}Fe_{0.35}$@PCN before (solid curve) and after (dash curve) stability test in O_2-satuated 1 M KOH without IR-correction. Scan rate: 10 mV/s, electrode rotation rate: 1600 rpm. Stability test: chronoamperometry at 1.53 V (vs. RHE) for 2 h in O_2-satuated 1 M KOH.

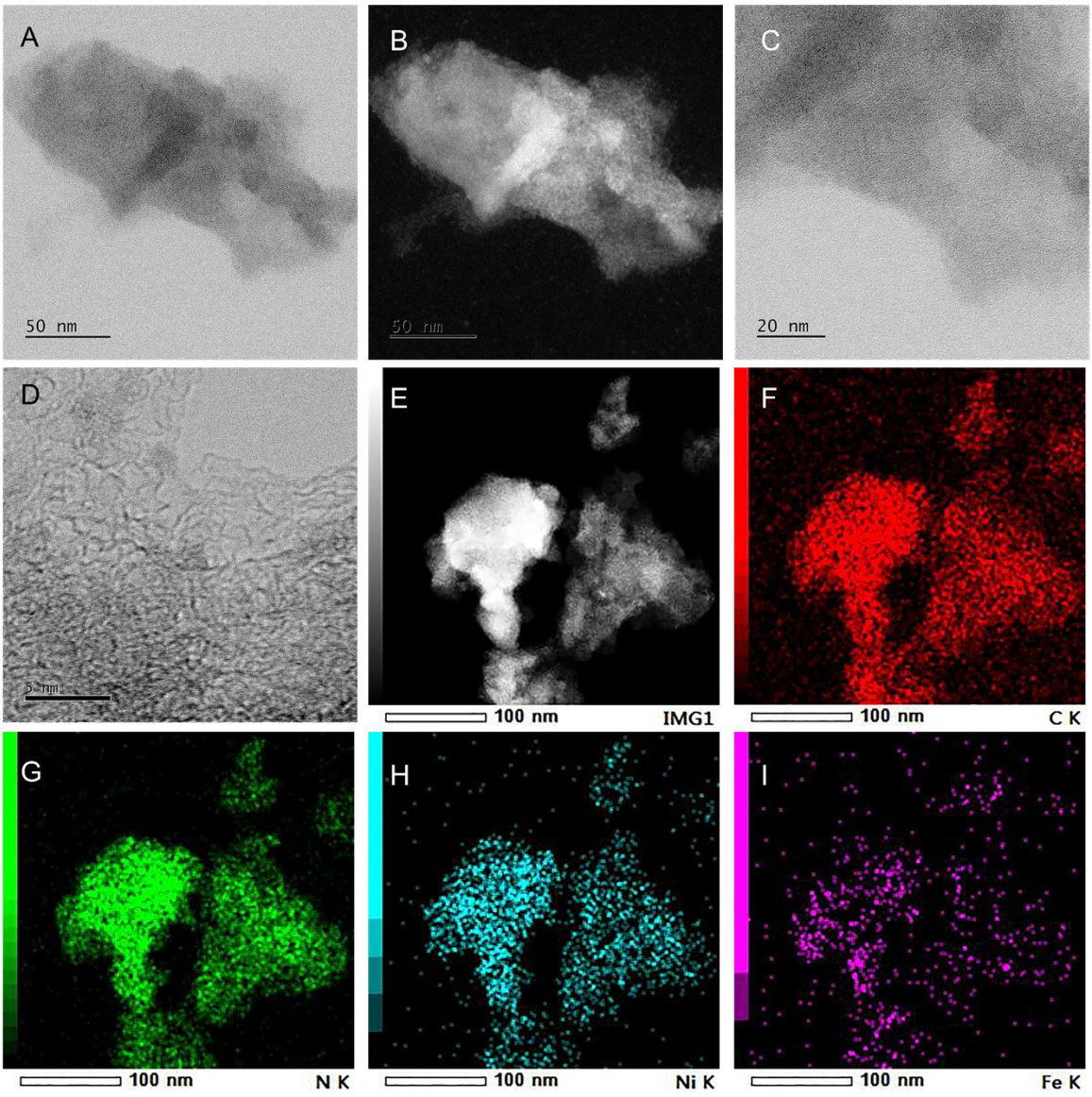

Figure S14. TEM images of $Ni_{0.65}Fe_{0.35}$@PCN after OER test as well as corresponding EDS mapping images of C, N, Ni and Fe.

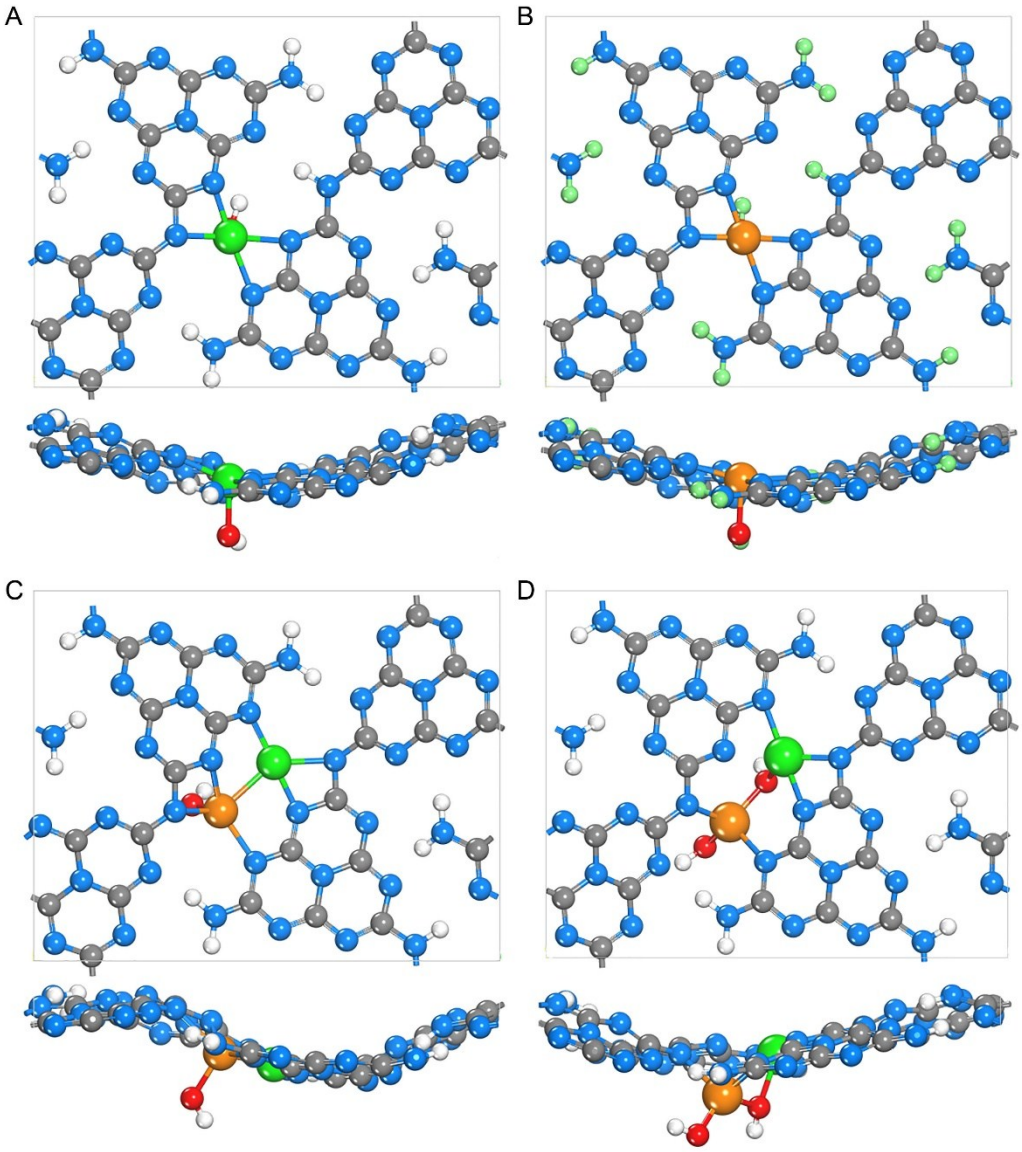

Figure S15. Top and side views of four different configurations of NiOH@PCN (A), FeOH@PCN (B), NiFeOH@PCN (C), and $NiFe(OH)_2$@PCN (D) after geometry optimization. The green, yellow, red, blue, gray and white balls are Ni, Fe, O, N, C and H atoms, respectively.

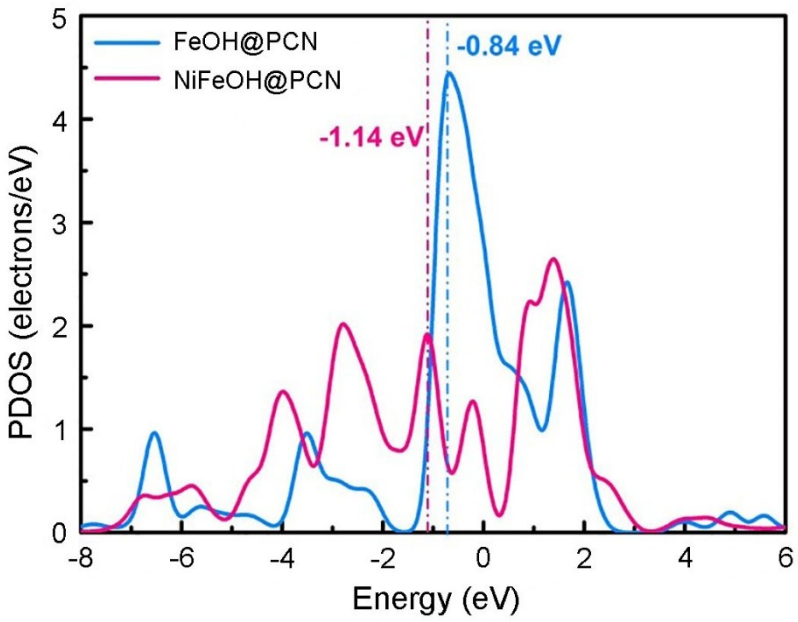

Figure S16. The density of states and d band center of Fe atoms in FeOH@PCN and NiFeOH@PCN.

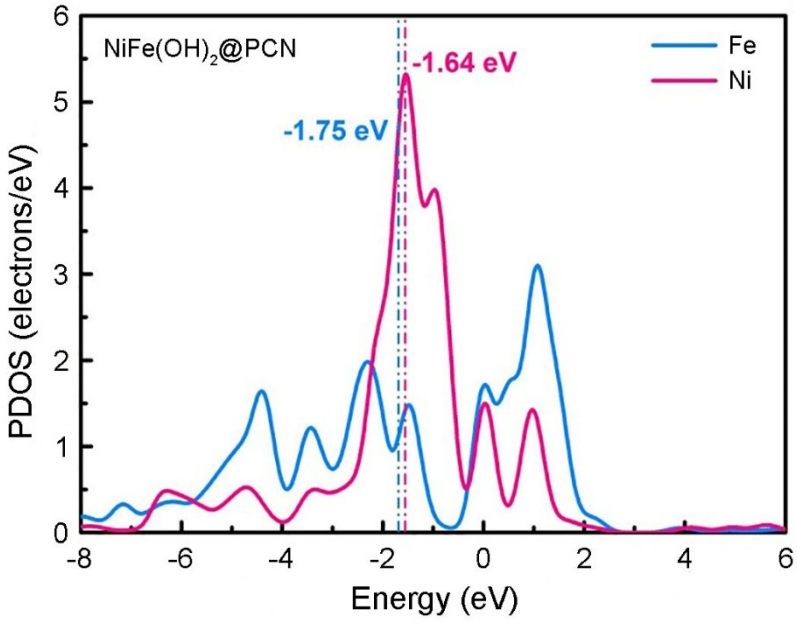

Figure S17. The density of states and d band center of Fe and Ni atoms in $NiFe(OH)_2$@PCN.

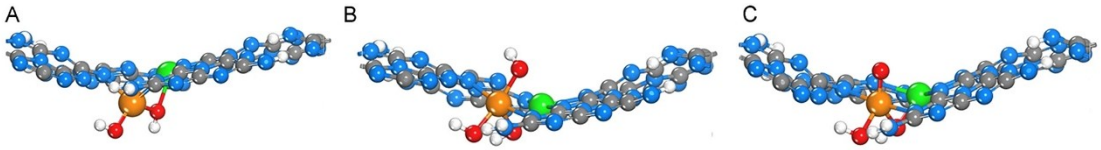

Figure S18. The bare $NiFe(OH)_2$@PCN substrate (A) and with adsorbed OH* (B) and O* (C) after geometry optimization. The green, yellow, red, blue, gray and white balls are Ni, Fe, O, N, C and H atoms, respectively.

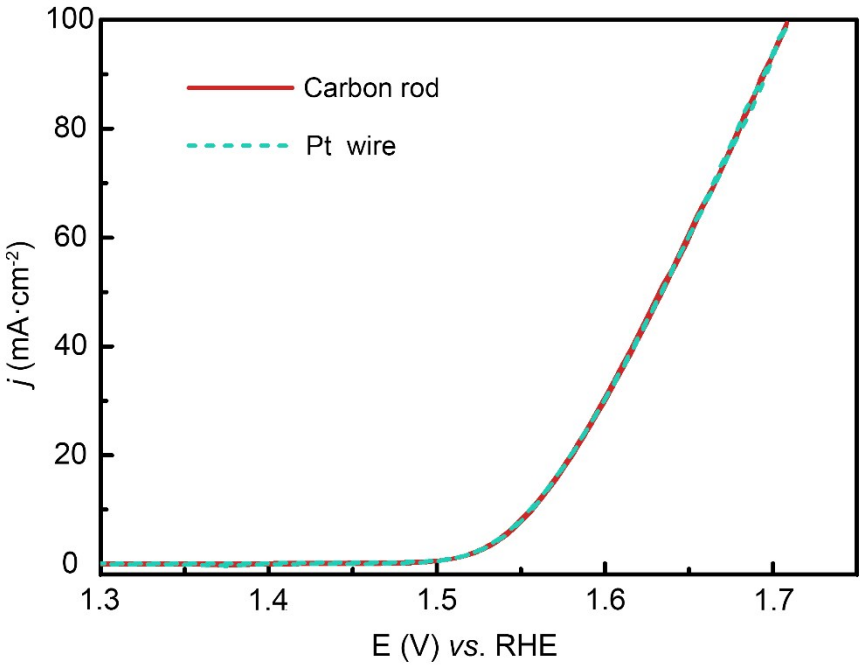

Figure S19. OER polarization curves of $Ni_{0.65}Fe_{0.35}$@PCN with carbon rod and Pt wire as counter electrode, respectively. Experiments was conducted in O_2-satuated 1 M KOH without IR-correction. Scan rate: 10 mV/s, electrode rotation rate: 1600 rpm.

II. Supplemental Tables

Table S1. The molar ratio of Ni/(Ni+Fe) in Ni_xFe_{1-x}@PCN.

Ni/(Ni+Fe) (Molar ratio)	$Ni_{0.22}Fe_{0.78}$@PCN	$Ni_{0.43}Fe_{0.57}$@PCN	$Ni_{0.65}Fe_{0.35}$@PCN	$Ni_{0.82}Fe_{0.18}$@PCN
reactants	0.20	0.35	0.50	0.80
ICP-OES	0.22	0.43	0.65	0.82

Table S2. XPS analysis of Ni_xFe_{1-x}@PCN and PCN

Element	Type of bonding	Catalyst	Binding energy
Carbon (C 1s)	C-C	For all	284.5 eV
	R-OH or C-O-C	For all	285.5 eV
	C≡N; sp-hybridized carbon	For all	286.5 eV
	N-C=N; sp^2-hybridized carbon	x = 0	287.9 eV
		x = 0.65	287.7 eV
		x = 0.82	287.7 eV
		x = 1	287.8 eV
	C(O)-O-C or COOH	For all	289.2 eV
Nitrogen (N 1s)	C-N=C; sp^2-hybridized nitrogen	PCN	398.5 eV
		x = 0	398.4 eV
		x = 0.65	398.3 eV
		x = 0.82	398.4 eV
		x = 1	398.4 eV
	$N-(C)_3$; sp^3-hybridized nitrogen	PCN	399.8 eV
		x = 0	399.8 eV
		x = 0.65	399.7 eV
		x = 0.82	399.9 eV
		x = 1	399.7 eV
	$C-NH_x$ or C≡N; primary/secondary amine or cyano group	For all	401.0 eV

Table S3. EXAFS data fitting results of Fe@PCN and $Ni_{0.65}Fe_{0.35}$@PCN for Fe K-edge

Sample	Fe-N CN[a]	R[b] / Å	$(\sigma^2)^c*10^2$ / $Å^2$	ΔE_0[d] / eV
Fe@PCN	2.5 ± 0.2	2.039 ± 0.007	0.737 ± 0.060	5.7
$Ni_{0.65}Fe_{0.35}$@PCN	2.7 ± 0.5	2.016 ± 0.018	0.863 ± 0.207	10.0

[a] CN: coordination number.

[b] R: interatomic distance.

[c] σ^2: Debye-Waller factor.

[d] E_0: energy shift.

Table S4. EXAFS data fitting results of Ni@PCN and $Ni_{0.65}Fe_{0.35}$@PCN for Ni-K edge including coordination number (CN), interatomic distance (R), Debye-Waller factor (σ^2), and energy shift (E_0).

Sample	Ni-N CN[a]	R[b] / Å	$(\sigma^2)^c*10^2$ / $Å^2$	ΔE_0[d] / eV
Ni@PCN	2.1 ± 0.3	1.86 ± 0.02	0.41 ± 0.26	6.2
$Ni_{0.65}Fe_{0.35}$@PCN	2.9 ± 0.2	1.87 ± 0.01	0.56 ± 0.13	6.4

[a] CN: coordination number.

[b] R: interatomic distance.

[c] σ^2: Debye-Waller factor.

[d] E_0: energy shift.

Table S5. E_0[a] Values of the NiFe@PCN as well as reference samples.

Sample	Fe foil	Fe Pc	Fe@PCN	$Ni_{0.65}Fe_{0.35}$@PCN
E_0 for Fe (eV)	7112	7122.5	7120.2	7122.4
Sample	Ni foil	Ni Pc	Ni@PCN	$Ni_{0.65}Fe_{0.35}$@PCN
E_0 for Ni (eV)	8333	8339.1	8338.7	8338.7

[a]E_0: the first inflection point.

Table S6. The zero point energies and entropic corrections of oxygenates at 298 K

Species	ZPE[1]	TS[1]	ZPE[2]	TS[2]	ZPE[a]	TS[a]
O*	0.05	0.00	0.084	0.05	0.13	0.04
OH*	0.36	0.06	0.386	0.07	0.39	0.09
OOH*	0.40	0.08	0.457	0.16	0.49	0.13
O_2	0.11	0.64	-	-	-	-
H_2	0.27	0.41	0.27	0.41	0.27	0.41
H_2O	0.56	0.67	0.56	0.67	0.56	0.67

[a] The present work.

Table S7. The free energy of adsorbed oxygenates at 298 K

	NiOH@PCN	FeOH@PCN	NiFeOH@PCN	$NiFe(OH)_2$@PCN
ΔG_{OH*}	0.94	-0.26	0.36	1.34
ΔG_{O*}	2.95	0.99	1.16	2.32
ΔG_{OOH*}	3.78	2.63	3.24	4.00

Table S8. The reaction free energy ΔG of NiOH@PCN, FeOH@PCN, NiFeOH@PCN, and $NiFe(OH)_2$@PCN

NiOH@PCN	U = 0	U = 1.23	U = 1.58
$\Delta G_1 = \Delta G_{OH^*} - eU$	0.94	-0.29	-0.64
$\Delta G_2 = \Delta G_{O^*} - \Delta G_{OH^*} - eU$	2.01	0.78	0.43
$\Delta G_3 = \Delta G_{OOH^*} - \Delta G_{O^*} - eU$	0.83	-0.40	-0.75
$\Delta G_4 = 4.92 - \Delta G_{OOH^*} - eU$	1.14	-0.09	-0.44
FeOH@PCN	U = 0	U = 1.23	U = 1.58
$\Delta G_1 = \Delta G_{OH^*} - eU$	-0.26	-1.49	-1.84
$\Delta G_2 = \Delta G_{O^*} - \Delta G_{OH^*} - eU$	1.25	0.02	-0.33
$\Delta G_3 = \Delta G_{OOH^*} - \Delta G_{O^*} - eU$	1.64	0.41	0.06
$\Delta G_4 = 4.92 - \Delta G_{OOH^*} - eU$	2.30	1.07	0.72
NiFeOH@PCN	U = 0	U = 1.23	U = 1.58
$\Delta G_1 = \Delta G_{OH^*} - eU$	0.36	-0.87	-1.22
$\Delta G_2 = \Delta G_{O^*} - \Delta G_{OH^*} - eU$	0.81	-0.42	-0.77
$\Delta G_3 = \Delta G_{OOH^*} - \Delta G_{O^*} - eU$	2.08	0.85	0.50
$\Delta G_4 = 4.92 - \Delta G_{OOH^*} - eU$	1.68	0.45	0.10
$NiFe(OH)_2$@PCN Path I	U = 0	U = 1.23	U = 1.58
$\Delta G_1 = \Delta G_{OH^*} - eU$	1.34	0.11	-0.24
$\Delta G_2 = \Delta G_{O^*} - \Delta G_{OH^*} - eU$	0.98	-0.25	-0.60
$\Delta G_3 = \Delta G_{OOH^*} - \Delta G_{O^*} - eU$	1.68	0.45	0.10
$\Delta G_4 = 4.92 - \Delta G_{OOH^*} - eU$	0.92	-0.31	-0.66
$NiFe(OH)_2$@PCN Path II	U = 0	U = 1.23	U = 1.58
$\Delta G_1 = \Delta G_{OH^*} - eU$	1.34	0.11	-0.24
$\Delta G_2 = \Delta G_{O^*} - \Delta G_{OH^*} - eU$	0.98	-0.25	-0.60
$\Delta G_3 = \Delta G_{O^*+OH^-} - \Delta G_{O^*} - eU$	0.80	-0.43	-0.78
$\Delta G_4 = 4.92 - \Delta G_{O^*+OH^-} - eU$	1.80	0.57	0.22

III. Supplemental Details of Calculation Method

The adsorption free energy of intermediate species are determined using[3] $\Delta G_{ads} = \Delta E_{ads}^{DFT} + \Delta ZPE - T\Delta S$, where ΔE_{ads}^{DFT} can be calculated relative to H_2O and H_2. The absorption energies were calculated as follows, $\Delta E_{OH^*} = E(OH^*) - E(*) - (E_{H_2O} - 1/2E_{H_2})$, $\Delta E_{OOH^*} = E(OOH^*) - E(*) - (2E_{H_2O} - 3/2E_{H_2})$, $\Delta E_{O^*} = E(O^*) - E(*) - (E_{H_2O} - E_{H_2})$, E_{H_2O} and E_{H_2} are the calculated DFT energies of H_2O and H_2 molecules in the gas phase using the approaches outlined by Nørskov et al.[3, 4] ΔZPE and $T\Delta S$ are the zero point energy difference and the entropy change between the absorbed state and the free state, i.e., the gas phase (listed in Table S6), respectively, and $T\Delta S$ is the temperature (298.15 K in this work). Because the high-spin ground state of an oxygen molecule is difficult to describe in DFT calculations, the free energy of $O_2(g)$ is derived as $G_{O_2}(g) = 2G_{H_2O}(l) - 2G_{H_2}(g) + 4.92eV$.

For each step, the reaction free energy ΔG is defined as the difference between free energies of the initial and final states and is given by the expression,[5]

$$\Delta G = \Delta E + \Delta ZPE - T\Delta S + \Delta G_U$$

Here ΔE is the reaction energies obtained from DFT total energies of the catalyst surface with possible configurations of adsorbed reactants or intermediates. If a reaction step involves the electron and proton transfer, the relevant bias effects are taking into account by shifting the energy by $\Delta G_U = -eU$, where U is the electrode potential and e is a transferred charge.

REFERENCES

1 S. Zhou, N. Liu, Z. Wang and J. Zhao, *ACS Appl. Mater. Interfaces*, 2017, **9**, 22578-22587.

2 M. Li, L. Zhang, Q. Xu, J. Niu and Z. Xia, *J. Catal.*, 2014, **314**, 66-72.

3 J. K. Nørskov, J. Rossmeisl, A. Logadottir, L. Lindqvist, J. R. Kitchin, T. Bligaard and H. Jónsson, *J. Phys. Chem. B*, 2004, **108**, 17886-17892.

4 I. C. Man, H.-Y. Su, F. Calle-Vallejo, H. A. Hansen, J. I. Martínez, N. G. Inoglu, J. Kitchin, T. F. Jaramillo, J. K. Nørskov and J. Rossmeisl, *ChemCatChem*, 2011, **3**, 1159-1165.

5 N. Yang, L. Li, J. Li, W. Ding and Z. Wei, *Chem. Sci.*, 2018, **9**, 5795-5804.